
Ultra-high Resolution SPECT System Using Four Pinhole Collimators for Small Animal Studies

Koichi Ishizu, Takao Mukai, Yoshiharu Yonekura, Marco Pagani, Toru Fujita, Yasuhiro Magata, Sadahiko Nishizawa, Nagara Tamaki, Hiroshi Shibasaki and Junji Konishi

Departments of Nuclear Medicine and Brain Pathophysiology, Faculty of Medicine, Kyoto University, Shogoin, Sakyo-ku, Kyoto, Japan

We describe a newly developed ultra-high resolution SPECT system using four pinhole collimators for small animal studies. **Methods:** The system utilizes a clinical four-head SPECT scanner with specially designed pinhole collimators. Four types of pinholes with different configurations were designed with different effective aperture sizes (1.0, 2.0 and 4.0 mm) and rotating radii (40 mm and 50 mm). The distance from the axis of rotation to the scintillator was fixed to 180 mm. A filtered backprojection algorithm was used to reconstruct SPECT images after fan-beam-to-parallel-beam data conversion. **Results:** The system provided a reconstructed spatial resolution of 1.65 mm (FWHM) and sensitivity of 4.3 kcps/ μ Ci/ml with the best type of pinholes, respectively. The ^{99m}Tc -HMPAO SPECT image in rat studies clearly visualized small brain structures, and the left ventricular myocardium and cardiac cavity were clearly separated with ^{99m}Tc -MIBI. Dynamic SPECT imaging of rat brain with [^{123}I]iomazenil was also feasible. **Conclusion:** This ultra-high resolution SPECT system can be used to measure the regional distribution of radiolabeled tracers in small animals in vivo and may play a significant role in the development of new radiopharmaceuticals and in studies of various disease models using living animals.

Key Words: single-photon-emission computed tomography; pinhole collimator; ultra-high resolution

J Nucl Med 1995; 36:2282-2287

Increasing interest in physiological and biochemical imaging with SPECT stimulates the development of new ^{99m}Tc or ^{123}I -labeled radiopharmaceuticals. Regional distribution of these compounds needs to be evaluated in small animals before further studies in larger animals or clinical applications.

The studies of new radiopharmaceuticals are usually performed by excision and direct counting of selected organs and by macroautoradiography to obtain higher spatial resolution (1,2). The disadvantage of these meth-

ods is that the animals have to be killed to obtain the measurements. Many animals are used to estimate temporal changes in tissue distribution and even more animals are required for more accurate measurements. Moreover, follow-up studies after a sufficient interval are not possible in the same animal, and it is often difficult to obtain several samples, especially when animal disease models are used.

Serial dynamic image analysis in living animals is extremely important when evaluating the kinetic behavior of radiolabeled compounds. Although such dynamic analysis can be performed on planar images in small animal studies, it cannot separate the radioactivity in the small structures overlapping each other (for example, between the cortex and deep gray matter, liver and liver tumors and myocardium and cardiac cavity). For this reason, SPECT imaging is ideal as it can separate these structures if sufficient spatial resolution is obtained.

Parallel-hole collimators can be used for high-resolution imaging of small animals, but the sensitivity would be very low. As in human brain imaging, fanbeam collimators may be applicable for small animals, but higher costs are a consideration. Recently, some groups have reported pinhole SPECT systems with excellent spatial resolution for small animal studies (3-5).

Pinhole collimators are constructed simply and can enable high-resolution imaging because of easily available geometric magnification. Pinhole collimation has been used for planar imaging of small human organs, such as the thyroid or adrenal glands, bone and kidneys, as well as small animals, although some distortion in image linearity exists in the peripheral area of the field of view (6-8). Vogel et al. reported a seven-pinhole system for multiplanar emission tomography in human study in 1978 (9), but a practical pinhole SPECT system was not developed for many years. Current pinhole SPECT systems (3-5) have relatively low sensitivity because a single-head camera is used. To obtain high spatial resolution in small animal studies, system sensitivity is sacrificed and more radioactivity or long acquisition times would be needed for practical imaging. Furthermore, in dynamic studies, long acquisition times cannot be used. To obtain both high resolution and high sensitivity and to adjust to different situations in animal stud-

Received Aug. 1, 1994; revision accepted Dec. 19, 1994.

For correspondence or reprints contact: Koichi Ishizu, MD, Department of Nuclear Medicine, Kyoto University Hospital, Shogoin, Sakyo-ku, Kyoto, 606-01 Japan.

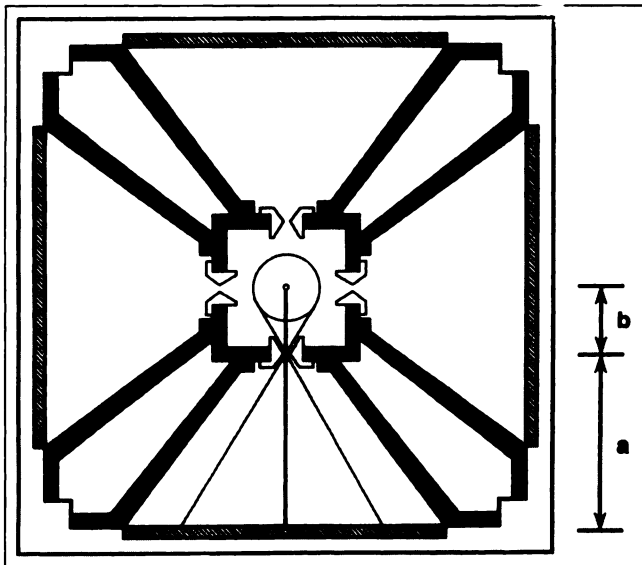


FIGURE 1. Schematic of four-head pinhole SPECT system consisting of four scintillators (shaded lines), four tungsten pinholes (white), four lead shields and a pinhole adapter (black). The distance from scintillator to pinhole (a) was 130 or 140 mm and the distance from the pinhole to the axis of rotation (b) was 50 or 40 mm, respectively.

ies, we applied exchangeable pinhole collimators with different dimensions to a four-head SPECT system.

This study reports the theoretical and practical evaluation of this newly developed SPECT system with four pinhole collimators.

METHODS

System Configuration

System resolution (R_s) of pinhole SPECT is a function of the geometric resolution (R_g) of the pinhole collimator and the intrinsic resolution (R_i) of the scintillation detector as shown by Equations 1 and 2. The sensitivity of pinhole SPECT can be calculated according to Equation 3.

$$R_s^2 = R_g^2 + (b/a)^2 R_i^2 \quad \text{Eq. 1}$$

$$R_g = de(a + b)/a \quad \text{Eq. 2}$$

$$S = k \cdot de^2/b^2, \quad \text{Eq. 3}$$

where a = distance from scintillator to pinhole; b = distance from pinhole to axis of rotation; $R_i = 3.0$ mm for the SPECT-2000H system; S = system sensitivity; k = constant; and de = effective aperture of pinhole.

We used the SPECT-2000H scanner (Hitachi Medical Co., Tokyo, Japan). This system has four scintillators with NaI crystals sized $260 \times 208 \times 9$ mm and 120 photomultiplier tubes. Because all scintillators are connected firmly to each other by metal frames, the distance from the axis of rotation to the front surface of each scintillator is fixed to 180 mm. The intrinsic spatial resolution of this scintillator is 3.0 mm FWHM. The pinhole collimator consists of cone-shaped lead shields, tungsten pinholes and an attachment adapter as shown in Figure 1. Cone-shaped lead shields are firmly fixed to the scintillator using the mechanical attachment equipped for parallel-hole collimators. Tungsten pinholes are exchangeable to the attachment adapter and the

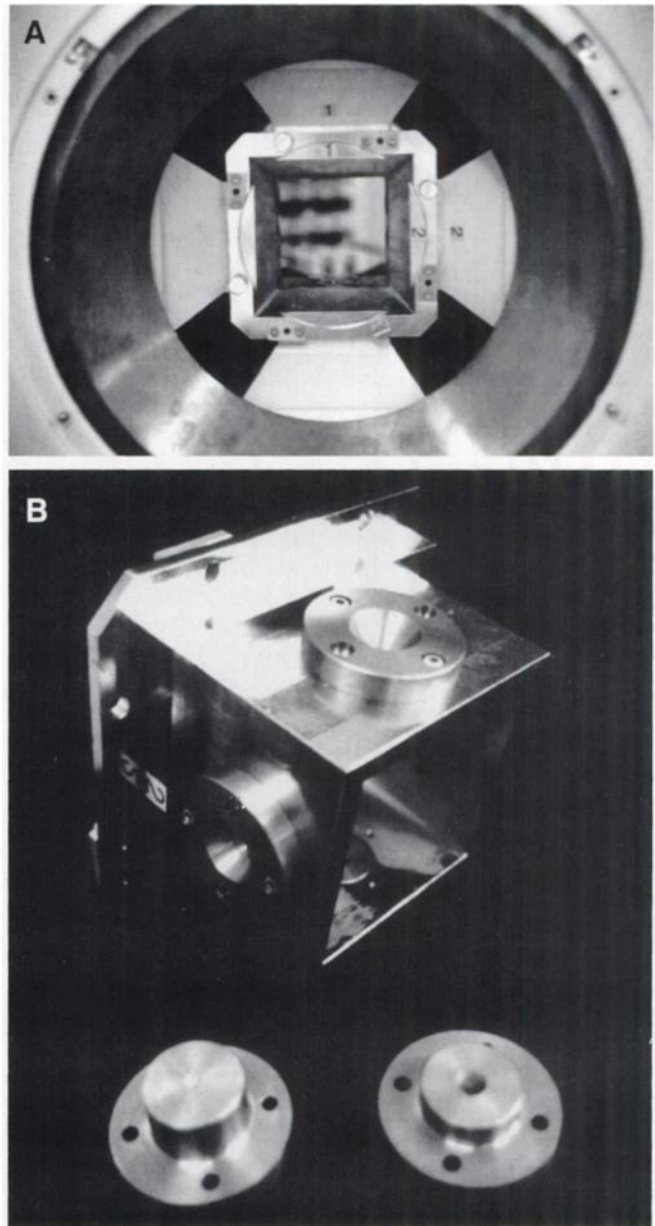


FIGURE 2. Four-head pinhole SPECT system. (A) Gantry. Pinhole collimators are attached to the four-head SPECT camera. (B) Pinhole adapter and two different types of pinholes.

distance between pinhole to the axis of rotation can be changed by using pinholes with a different height. Figure 2 shows the system before it is attached to the four-head SPECT camera. Four different types of pinholes were designed. Aperture sizes and rotation radii were 1.0 and 40 mm, 1.0 and 50 mm, 2.0 and 50 mm and 4.0 and 50 mm, respectively. The field of view was 50 mm in diameter and 32.6 mm in the axial direction with a minimum slice thickness of 0.51 mm when the pinhole rotating radius was 50 mm (Table 1).

Data Acquisition and Reconstruction

Projection data can be obtained using a 128×128 or 64×64 acquisition matrix in step-and-shoot mode with 128, 64 or 32 views over 360° or in continuous rotating mode over 360° . Data acquisition, fanbeam-to-parallel-beam data conversion, image reconstruction and image display were performed using a mini-computer connected to the scintillation detectors.

TABLE 1
Geometry, Sensitivity and Spatial Resolution of the SPECT System with Four Types of Pinhole Collimators

Collimator	Pinhole aperture (mm)	Rotation radius (mm)	Diameter of FOV (cm)	System sensitivity (kcps/ μ Ci/ml)	Spatial resolution (mm; FWHM)
Pinhole 1	1.0 (1.2*)	40	3.7	0.60	1.65
Pinhole 2	1.0 (1.2*)	50	5.0	0.39	1.96
Pinhole 3	2.0 (2.2*)	50	5.0	1.19	2.80
Pinhole 4	4.0 (4.2*)	50	5.0	4.29	4.15

*Effective aperture of pinhole (mm).

Sensitivity compensation was performed for the raw data by normalizing the solid angle between the incident gamma-ray and the scintillator using the following equation:

$$A = A_m \cdot \sin^{-3} \theta, \quad \text{Eq. 4}$$

where A = compensated activity and A_m = measured activity.

For the compensated raw data, fanbeam-to-parallel-beam data conversion, similar to a fanbeam collimator SPECT system, was performed prior to SPECT image reconstruction by a filtered backprojection algorithm. To obtain the parallel-beam pixel configuration, pixels were interpolated from raw fanbeam data. A ramp filter was used for phantom studies and a Shepp-Logan filter was used for animal studies. Corrections for radionuclide decay, attenuation or scatter were not performed.

Phantom Experiments

Spatial resolution and system sensitivity were obtained through different pinhole collimators. A line source phantom was made using glass tubes (60 mm length \times 0.26 mm inner diameter) filled with [^{99m}Tc]pertechnetate solution (40 mCi/ml). For spatial resolution measurements, five parallel glass tubes were placed 5 or 10 mm apart in one plane. To check the distortion in the reconstructed image, 89 parallel glass tubes were placed 4 mm from each other in the field of view. A cylindrical phantom (4.8 mm inner diameter) containing homogeneous concentration of ^{99m}Tc was placed on the axis of rotation to determine system sensitivity. The measurements were performed in a phantom section in case the gamma-ray released from the section was projected on the scintillator at an angle of 90° . In all measurements, data acquisition was performed with four scintillation detectors, and all types of pinhole collimators were tested and compared. For all phantom studies, projection data were acquired from 128 views over 360° using a 128×128 matrix and a 20% (126–154 keV) energy window.

Animal Experiments

Male Wistar rats were studied. For brain imaging, 7 mCi ^{99m}Tc -hexamethyl-propyleneamine oxime (HMPAO) were injected intravenously 30 min before imaging and data were acquired for 96 min. For heart studies, a 64-min scan was obtained starting 70 min postinjection of 9 mCi ^{99m}Tc -methoxyisobutyl isonitrite (MIBI). Each rat was anesthetized by sodium pentobarbital and kept alive throughout the scan sequence. In both studies, pinhole collimators with a 1.0-mm aperture and 50-mm rotation radius were used. Projection data were acquired from 128 views over 360° using a 128×128 matrix in a 20% (126–154 keV) energy window.

For dynamic data acquisition in the brain studies, [^{123}I]iomazenil, a SPECT ligand for CNS benzodiazepine receptors (10), was used. After intravenous injection of 4.5 mCi [^{123}I]iomazenil, nine SPECT scans of 15 min each (total 135 min) were obtained using pinholes

with a 1.0-mm aperture and a 40-mm rotation radius. Data were acquired with 128×128 acquisition matrix and 64 acquisition steps. In one study, 0.5 and 1.0 mg diazepam were injected intravenously at 60 and 90 min postinjection of iomazenil, respectively. Diazepam was not given to the other two rats. Regions of interest (ROIs) were placed on the representative area of the cerebral cortex and striatum on the reconstructed images. Background counts (the mean counts of the area out of the rat body) were subtracted in each image, and the counts in ROIs were normalized by the maximum count of the cortex.

RESULTS

Spatial Resolution and Image Distortion

Comparison between the measured spatial resolution (FWHM for SPECT images) for each pinhole collimator configuration is shown in Table 1. The highest spatial resolution was 1.65 mm (FWHM) with 1.0-mm aperture and 40-mm rotation radius pinholes. No large variations in the spatial resolutions of the SPECT images were observed at several off-center locations. Figure 3 shows the profile curves of the line source phantom.

The reconstructed image of the 89-line source phantom with [^{99m}Tc]pertechnetate solution is shown in Figure 4. All line sources, 4 mm apart from each other, were clearly visualized, although a small distortion of image linearity was seen in the peripheral area of the reconstructed image.

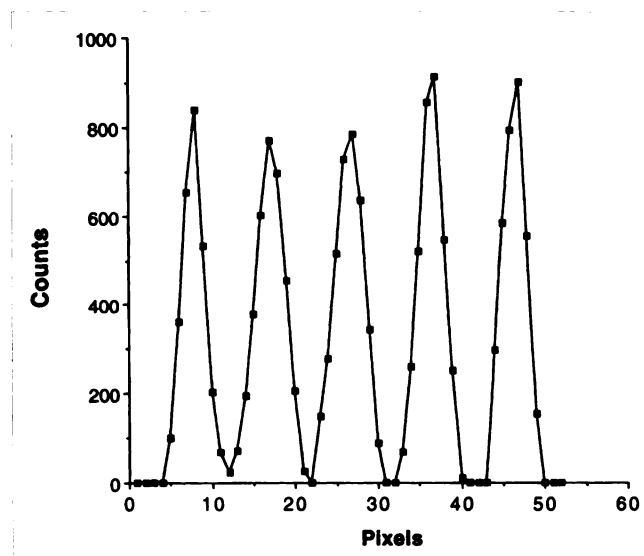


FIGURE 3. The profile curve of five-line sources phantom image with a 1.0-mm aperture and 50-mm rotation radius pinhole collimators. The distance between each source is 5 mm.

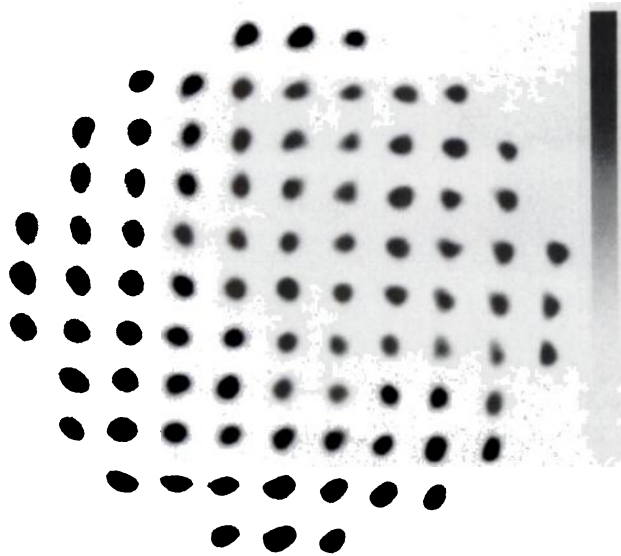


FIGURE 4. Reconstructed image of a line source phantom with 89 glass tubes. The distance between each line sources is 4 mm. All line sources were clearly visualized and image linearity distortion was small.

System Sensitivities

Table 1 shows the sensitivities of the SPECT system with four types of pinhole collimators measured by the cylindrical phantom. The sensitivities were measured on a phantom section at the center of the field of view. System sensitivity with the 4.0-mm aperture pinholes was 4.29 kcps/ μ Ci/ml. Figure 5 demonstrates the high linear correlation between the measured sensitivity of the system and the theoretical estimation of the relative sensitivity changes due to the difference in the effective aperture of the pinhole collimators and the distance from the axis of rotation to the pinhole.

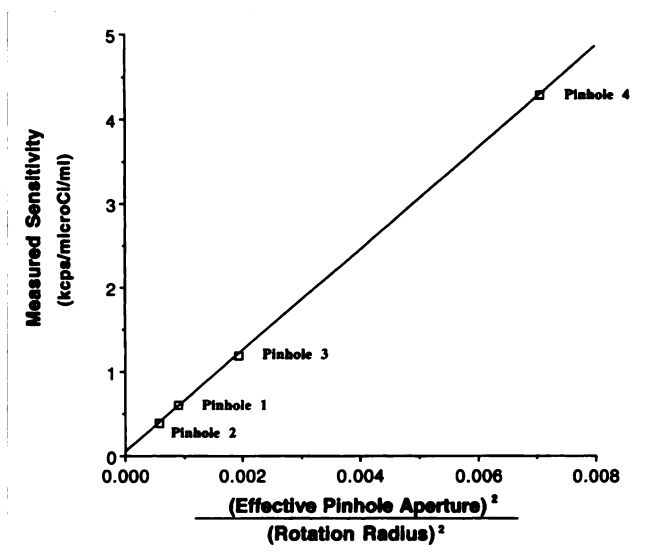


FIGURE 5. Measured sensitivity with pinhole collimators of different aperture size. Theoretically, the sensitivity is in proportion to the square of the effective pinhole aperture and in inverse proportion to the square of the distance from the pinhole to the axis of rotation (Eq. 3).

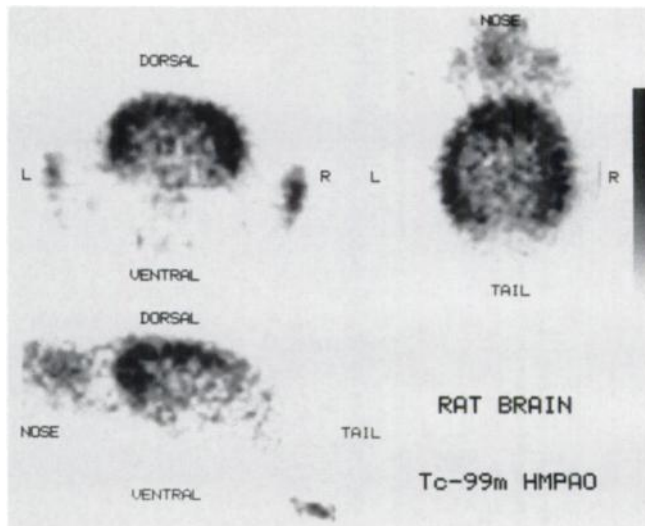


FIGURE 6. Brain perfusion ^{99m}Tc -HMPAO SPECT images in the rat.

Animal Scans

Figures 6 and 7 show the perfusion images of the rat brain and myocardium obtained with ^{99m}Tc -HMPAO and ^{99m}Tc -MIBI, respectively. The functional structures of the rat brain and the myocardium were clearly visualized.

Figure 8 shows serial dynamic SPECT [^{123}I]iomazenil images of the rat brain. Time-activity curves for [^{123}I]iomazenil in the cerebral cortex and striatum are shown in Figure 9. The radioactivity in both the cerebral cortex and striatum reached the maximum counts in the second frame (15–30 min postinjection) and decreased gradually thereafter, but the striatum showed a faster decrease, which correspond to the lesser density of benzodiazepine receptors. In addition, intravenous administration of diazepam accelerated iomazenil washout from the cerebral cortex.

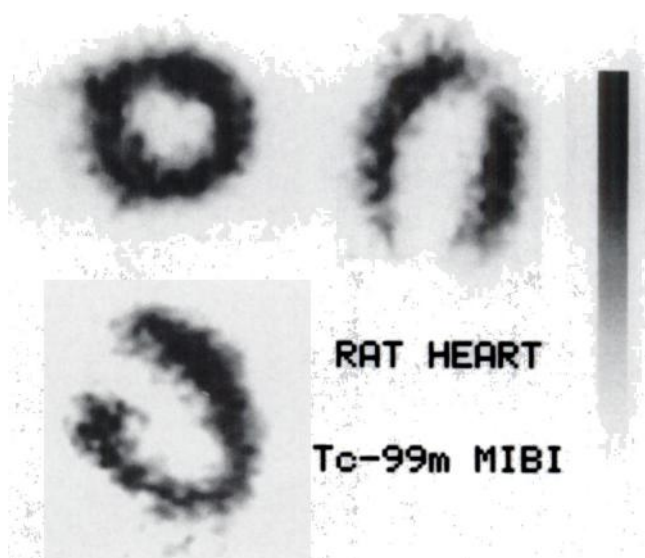


FIGURE 7. Myocardial perfusion ^{99m}Tc -MIBI SPECT images in the rat. Left ventricular wall and cardiac cavity are clearly visualized.

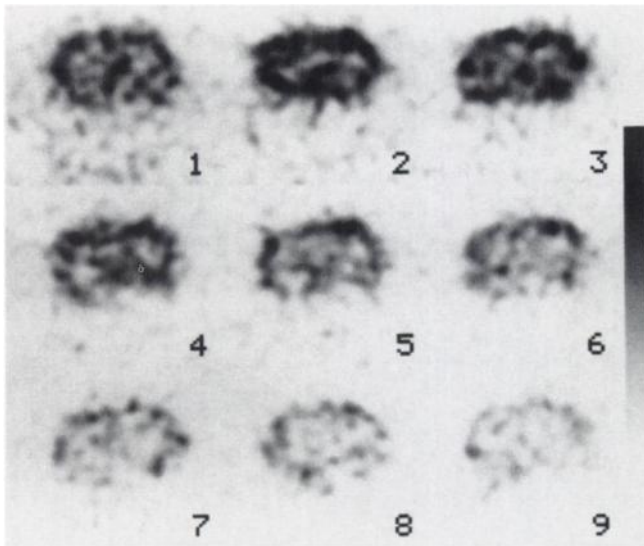


FIGURE 8. Serial dynamic [^{123}I]iomazenil SPECT images of the rat brain. Each image was acquired for 15 min postinjection.

DISCUSSION

In our theoretical and clinical evaluation of a newly developed SPECT system with four pinhole collimators, we obtained a spatial resolution of 1.65 mm (FWHM) when using four scintillation scanners. We used a four scintillation scanner system because high system sensitivity is extremely important in clinical studies. The excellent mechanical accuracy owes a great deal to the attachment adapter which firmly connects the four pinholes and four scintillation detectors to each other and assists in the accurate positioning between pinholes and detectors. The adapter system was also indispensable for exchanging pinholes of different dimensions. The system sensitivity was high enough to ob-

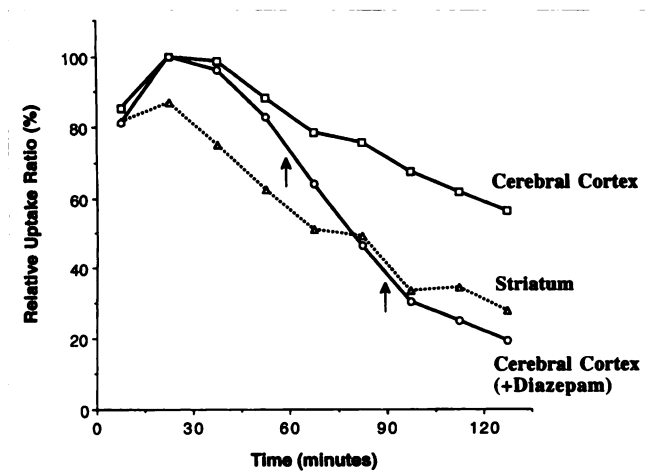


FIGURE 9. Temporal changes in radioactivity of [^{123}I]iomazenil in rat cerebral cortex and striatum (average of two rats). The counts in ROIs were normalized by the maximum counts in the cortex. The dotted line shows the radioactivity in the cortex of one rat given 0.5 and 1.0 mg of diazepam 60 and 90 min (p.i.), respectively. Diazepam decreased [^{123}I]iomazenil binding in the cerebral cortex, demonstrating the feasibility of this approach for kinetic analysis in rat brain.

tain a time-activity curve of the small structure of the rat on SPECT images. The time-activity curve of ^{123}I -iomazenil in rat cerebral cortex and striatum were in good agreement with the results of an in vivo quantitative autoradiographic study (11). As shown in Figure 7, the SPECT images could clearly visualize the rat myocardium and cardiac cavity. The possibility to distinguish two regions that cannot be separated in planar images is an important advantage of SPECT imaging.

Although the spatial resolution and system sensitivity were excellent in this study, we must describe that they would be worse if a wider field of view were required. Our pinhole SPECT system was designed to have a relatively small field of view (50 or 37 mm in diameter), which was considered to be sufficient to study rats or mice.

Pinhole SPECT cameras collect conebeam projection data through the pinhole collimator. To reconstruct SPECT images, a filtered backprojection algorithm with fanbeam-to-parallel-beam data conversion or a three-dimensional filtered backprojection algorithm, which was originally proposed by Feldkamp et al., is necessary (12). With the former algorithm, image distortion becomes greater when the distance from the sample section to the center of the field of view increases. On the other hand, the distortion can be neglected when this distance is small. Although the three-dimensional filtered backprojection method is ideal, we used the former algorithm, after which coronal, sagittal or oblique angle slice images were reorganized from the serial transaxial SPECT images.

Similar to other SPECT systems, our pinhole SPECT system has a limitation for quantitative measurement. Semiquantitative analysis, however, (e.g., using standardized uptake values) seems to be useful in determining regional distribution of administered tracer in small animals. The pinhole SPECT system is also being considered for use in high-resolution SPECT imaging of human organs, but the necessity of a long rotation radius for the human body or head may decrease its sensitivity markedly.

CONCLUSION

Our pinhole SPECT system collects data with sufficient resolution and sensitivity to image small animals and analyze dynamic changes in radioactivity. This system may play an important role in the development of new radiopharmaceuticals and in the study of various animal disease models.

ACKNOWLEDGMENTS

The authors thank Drs. H. Saji and Y. Fujibayashi for technical support and Miss A. Hashimoto for her help in preparing the manuscript.

REFERENCES

- Yonekura Y, Brill AB, Som P, Bennett GW, Fand I. Quantitative autoradiography with radiopharmaceuticals, part 1: digital film-analysis system by videodensitometry: concise communication. *J Nucl Med* 1983;24:231-237.
- Som P, Yonekura Y, Oster ZH, et al. Quantitative autoradiography with radiopharmaceuticals, part 2: applications in radiopharmaceutical research: concise communication. *J Nucl Med* 1983;24:238-244.
- Palmer J, Wollmer P. Pinhole emission computed tomography: method and experimental evaluation. *Phys Med Biol* 1990;35:339-350.
- Vaquero RA, Lowinger T, Strashun A. Transverse single-photon emission

computed tomography with a pinhole collimator [Abstract]. *J Nucl Med* 1987;28:678.

- Weber DA, Ivanovic M, Franceschi D, et al. Pinhole SPECT: an approach to in vivo high resolution SPECT imaging in small laboratory animals. *J Nucl Med* 1994;35:342-348.
- Hayes M. Is field size enlargement with divergent and pinhole collimators acceptable? *Radiology* 1970;95:525-528.
- Hurley PJ, Strauss HW, Pavoni P, Langan JK, Wagner HN. The scintillation camera with pinhole collimator in thyroid imaging. *Radiology* 1971;101:133-138.
- Sostre S, Ashare A, Quinones JD, et al. Thyroid scintigraphy: pinhole images versus rectilinear scans. *Radiology* 1978;129:759-785.

- Vogel RA, Kirch DL, LeFree MT, et al. A new method of multiplanar emission tomography using a seven pinhole collimator and an Anger camera. *J Nucl Med* 1978;19:648-654.
- Sybirka E, Al-Tikrit M, Zoghbi SS, et al. SPECT imaging of the benzodiazepine receptor: autoradiographic comparison of receptor density and radioligand distribution. *Synapse* 1992;12:119-128.
- Nagata T, Saji H, Nishizawa S, et al. Iodine-125-iomazenil binding in the brains of spontaneously epileptic rats: an ex vivo quantitative autoradiographic study. *Nucl Med Biol* 1995;22:445-449.
- Feldkamp LA, Davis LC, Kress JW. Practical cone-beam algorithm. *J Opt Soc Am* 1984;1:612-619.

EDITORIAL

Pinhole SPECT: Ultra-High Resolution Imaging for Small Animal Studies

Pinhole SPECT has recently been shown to provide a useful and inexpensive approach to obtaining high and ultra-high resolution images for small animal imaging (1-5). The use of small aperture pinhole collimators and short imaging distances for acquiring SPECT projection data can yield a system spatial resolution which is better than the intrinsic spatial resolution of the detector as a result of the large magnification factors (Fig. 1) which can be obtained with large field of view cameras (6,7). Since the resolution of pinhole collimators approaches the diameter of the pinhole aperture at small imaging distances, very high or ultra-high spatial resolution can be achieved using collimators with large magnification factors. Unfortunately, these gains in resolution are offset by large decreases in sensitivity; e.g., a 10-fold increase in resolution will result in a 100-fold decrease in sensitivity (Fig. 2). Compromises must be made between demands for spatial resolution and for sensitivity; however, this has not prevented its practical implementation for imaging. The initial reports on pinhole SPECT (1-5) were directed towards characterizing this new imaging technique and demonstrating the scope of potential applications for preclinical and research studies, with the potential for limited clinical applications. Of significance, especially in the current climate of increasing competi-

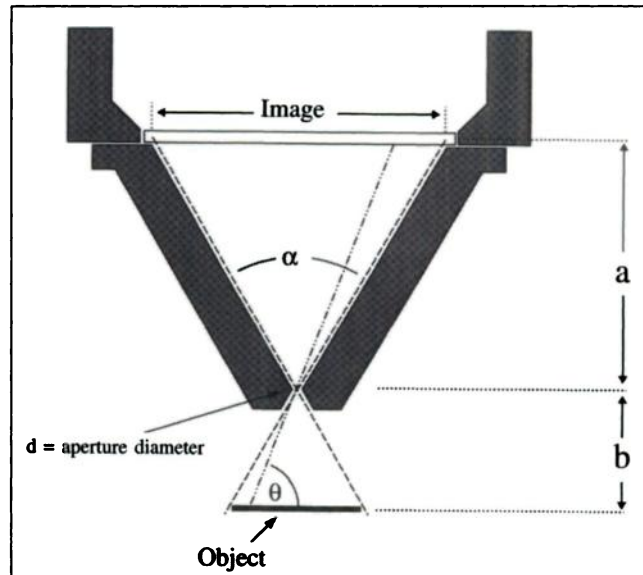


FIGURE 1. Imaging geometry for single pinhole collimator. Magnification of image projected on NaI(Tl) detector of pinhole collimated, scintillation camera is equal to ratio of distance, a , between detector and collimator aperture, to distance, b , between object which is imaged and collimator aperture. The geometric resolution of pinhole collimator, $R_g = [(a + b) d_0/a]$ and overall resolution, $R_o = [R_d^2 + (R_i b/a)^2]^{1/2}$, where R_d is intrinsic resolution of detector and d_0 is effective diameter of pinhole aperture. The effective diameter of pinhole collimator, d_0 , is larger than geometric diameter, d , as a result of penetration of edges of aperture by detected gamma rays, $d_0 = [d(d + 2/\mu \tan(\alpha/2))]^{1/2}$, where μ is linear attenuation coefficient of aperture material and α is acceptance angle of collimator. The geometric efficiency of pinhole collimator decreases in radial direction with $\sin^3\theta$ (6).

tion for a decreasing number of research dollars, is the accessibility of this technique to all institutions that have SPECT camera systems. The technique can be implemented by adding suitable reconstruction software to the conventional image processing software library and using appropriate small diameter pinhole collimator apertures for imaging. Pinhole SPECT, as an add-on to existing equipment, can provide the means for obtaining high-resolution

SPECT images at a fraction of the cost of the high-resolution imaging systems which have been designed for small animal imaging studies (8-10).

Extending the approach reported earlier for pinhole collimated, single-detector gamma camera SPECT systems (1-5), the article by Ishizu et al. in this issue of the *Journal* (11) shows that high-resolution tomographic slices can be obtained with a significant gain in sensitivity using a multicamera SPECT sys-

Received Jun. 6, 1995; accepted Aug. 15, 1995.
For correspondence or reprints contact: David A. Weber, PhD, Department of Radiology, U.C. Davis Medical Center, Folb II-E, 2421 45th St., Sacramento, CA 95817.